Electrodeposition of Bi_xFe_{1-x} Intermetallic Compound Nanowire Arrays and Their Magnetic Properties

Gao-Ren Li,*,† Ye-Xiang Tong,† Lin-Gang Kay,*,‡ and Guan-Kun Liu†

School of Chemistry and Chemical Engineering, Sun Yat-Sen University, Guangzhou 510275, China, and College of Engineering, University of Cincinnati, Cincinnati, Ohio 45219

Received: January 20, 2006; In Final Form: March 24, 2006

There have been few reports on Bi−Fe intermetallic compounds because Bi and Fe are immiscible in the equilibrium states and neither alloy nor intermetallic compound exists in the binary system. In this paper, we show that, by using the nanometer-scale templates based synthesis in conjunction with the electrochemical deposition, it is possible to mix in solid solution elements that are immiscible in traditional fabrication methods. The preparation of Bi−Fe intermetallic compound nanowire arrays was investigated via an electrodeposition route by using a polycarbonate (PC) membrane template. Cyclic voltammetry, potentiostatic transient, and potentiostatic stripping were used to study the formation of Bi_xFe_{1-x} intermetallic compounds. The compositions of $Bi_{1-x}Fe_x$ intermetallic compound nanowire arrays were sensitive to the bath compositions and the electrodeposition potentials, and the length could be easily adjusted by varying the electrodeposition time. The electrodeposited $Bi_{1-x}Fe_x$ intermetallic compound nanowire arrays had a parallel-to-the-wire easy magnetization. Furthermore, the spin-glass such as behavior and an unusually large characteristic time, which was about 5.26 h, were found in $Bi_{1-x}Fe_x$ intermetallic compound nanowire arrays at room temperature.

Introduction

Bismuth (Bi) is a semimetal with many unusual electronic properties that result from its low carrier concentrations, highly anisotropic Fermi surface, large Fermi wavelength, long carrier mean free path, and small effective carrier masses.[1−3] Because of these unusual properties, Bi-based intermetallic compounds have been extensively investigated for all kinds of functional materials.[4−6] For example, Bi−Sr−Ca−Cu and Bi−Pb−Sr−C−Cu intermetallic compounds are studied for superconducting materials, and bulk doped Bi_2Te_3 is studied currently for the most efficient thermoelectric material at 25 °C and a good target material for thermoelectric nanowires.[7] However, there has been few reports on Bi−Fe intermetallic compounds because Bi and Fe are immiscible in the equilibrium states and neither alloy nor intermetallic compound exists in the binary system.[8] It is considered to be very difficult to make Bi−Fe intermetallic compounds. However, we have recently discovered a very long relaxation time on the scale of more than 10 000 s at room temperature in Bi−transitional metal intermetallic compound systems.

Recently, the preparation and characterization of nanostructured Bi-based intermetallic compounds has became a hot theme in materials research.[9−14] Among various approaches to prepare nanostructured Bi-based intermetallic compounds, much attention has been paid to the nanometer-scale template-based synthesis in conjunction with electrochemical deposition because these templates possess a uniform porous structure. Arrays of nanowires are obtained by filling a polycarbonate template that contains a large number of straight cylindrical holes of uniform diameter. The method has been used to prepare both nanotubules and nanofibrils composed of conductive polymers, metals, semiconductors, carbon, and other materials.[15−17] As stimulated by the novel properties of carbon nanotubes, one-dimensional nanostructures are currently the subject of intense research because of the potential for nanoscale electronic and optoelectronic applications.[13,14] Despite its many unusual electronic properties, the synthesis of Bi−transitional metal intermetallic compound nanowires still cannot been seen in the literatures. Here, we present the preparation of Bi_xFe_{1-x} intermetallic compounds with nanowire array structure via the nanometer-scale template-based synthesis in conjunction with the electrochemical deposition in an organic bath. This simple and efficient method can be expected to be used in other systems that can be electrodeposited. Also, we investigated the magnetic relaxation phenomenon in the prepared Bi_xFe_{1-x} nanowire arrays and obtained an unusually large relaxation time.

2. Experimental Section

The electrochemical experiments were carried out in a simple three-electrode glass cell. The working electrodes were graphite, of an area 0.07 cm^2. A platinum foil with an area of 0.5 cm^2 was used as a counterelectrode, and a saturated calomel electrode (SCE) was used as the reference electrode, which was connected to the cell with a double salt bridge system. All potential values determined in this study were the values vs SCE.

The $E-t$ programs applied to the electrode were as follows: the potential was first switched from 0 to +0.8 V and maintained at +0.8 V for 2 min in order to clean the electrode surface. Electrodeposition was carried out with a potential in the range between −0.6 and −1.2 V, which is referred to as the electrodeposition potential E_c. For the stripping analyses, 0.1 M LiCl−DMF (*N*,*N*-dimethylformamide) was employed as the stripping media and the sweep rate was 0.10 V/s in all cases. Cyclic voltammetry, potentiostatic transient, and potentiostatic

* Corresponding authors. E-mail: ligaoren@yahoo.com.cn (G-R.L.).
† School of Chemistry and Chemical Engineering, Sun Yat-Sen University.
‡ College of Engineering, University of Cincinnati.

10.1021/jp060411n CCC: $33.50
Published on Web 04/15/2006

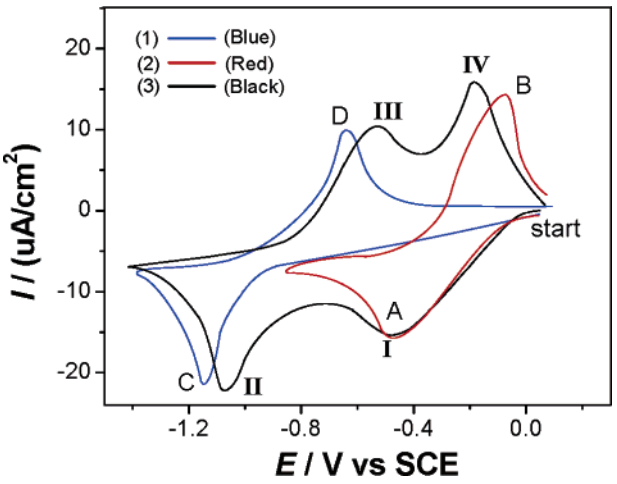

Figure 1. Cyclic voltammograms of the graphite electrodes in (1) 1 μM $FeCl_2$−DMF system; (2) 1 μM $Bi(NO_3)_3$−DMF system; (3) 1 μM $Bi(NO_3)_3$−1 μM $FeCl_2$−DMF system at 301 K.

stripping were done with a Zahner Elektrik IM6e electrochemical workstation.

The electrodeposition experiments were carried out in an organic bath containing $Bi(NO_3)_3$, $FeCl_2$, and DMF. Commercially available polycarbonate membranes (Whatman Inc.), with pore diameters of about 0.1 μm, pore density of about 4 $\times$ 10^9 pores/cm^2, and thickness of about 6−10 μm, were utilized as templates in this study. Before electrodeposition, a sputter deposition system (Cooke Vacuum Products, Inc., Norwalk, Conn.) with magnetron US gun (Mighty Mak Thin Film Products Inc.) and pulsed DC power supply (ENI RPG-50, Astec America, Inc.) was used, and a thin layer (25 nm) of iron was sputtered on the bottom side of the membranes to connect to the graphite electrode, and it acted as a working electrode. The prepared Bi_xFe_{1-x} intermetallic compound nanowire arrays were analyzed by X-ray energy dispersive spectroscopy (EDS) to determine the contents of bismuth and iron, and by X-ray diffraction (XRD) to determine the structures. The surface morphologies were observed with a field emission scanning electron microscope (FE-SEM). Superconducting quantum interference device (SQUID) measurements were carried out to investigate the magnetic behaviors of Bi_xFe_{1-x} intermetallic compound nanowire arrays.

3. Results and Discussion

Cyclic voltammetry was used to define the potential region for the deposition and dissolution of Bi_xFe_{1-x} intermetallic compound nanowire arrays. Figure 1(1) shows the cyclic voltammogram (CV) of 1 μM $Bi(NO_3)_3$−1 μM $FeCl_2$−DMF system at 301 K. The potential was scanned from the open circuit potential (0.06 V vs SCE) in the negative direction down to a potential of −1.42 V. It is clearly seen that the cathodic branch of the cyclic voltammogram exhibits two cathodic reduction peaks at approximately −0.48 V (peak I) and −1.07 V (peak II), respectively, as well as the anodic branch exhibiting two anodic oxidation peaks at −0.53 V (peak III) and −0.18 V (peak IV), respectively. According to the cyclic voltammograms of 1 μM $FeCl_2$−DMF and 1 μM $Bi(NO_3)_3$−DMF systems shown in Figure 1(1) and (2), respectively, peak I can be assigned to the electroreduction of Bi^{3+}. However, the potential of peak II that is at approximately −1.07 V is more positive than that of peak C, which corresponds to the bismuth deposition onto the graphite electrode. The shift of peak II in positive direction could be explained with the iron deposition on bismuth substrate formed during the deposition at the potential of peak I. Some amount of the deposited iron takes part in the formation of the solid solution Bi_xFe_{1-x}, but the rest of the deposited iron forms a separate pure iron phase. On the other hand, during the anodic scan, peak III can be assigned to the stripping of excess Fe from the Bi_xFe_{1-x} deposit. This CV also suggests that peak IV is the stripping of Bi_xFe_{1-x}, not Bi stripping as peak IV occurs at a potential less than 0.17 V positive to the potential of peak B. EDS elemental analysis of the electrodeposits formed in each solution also supports the above assignments.

Figure 2 shows the potentiostatic transients obtained from several potential steps of electrodeposition E_e (Figure 2a, c, e) and the corresponding stripping voltammetry analysis (Figure 2b, d, f) for the intermetallic compounds formed after the potential steps. In the case of the potential step carried out at an E_e= −0.60 V (Figure 2a), a potentiostatic transient that follows the Cottrell law is observed, with a charge value of 45 μC associated with the bismuth electrodeposition, as is demonstrated by the stripping voltammetry in Figure 2b, showing a single process corresponding to peak I in Figure 1(3). As we all know, the Cottrell law is applicable for the semi-infinite diffusion, and the electrodeposition to the pores should not follow the Cottrell law. However, a potentiostatic transient that follows the Cottrell law is observed. So we conclude that there is probably a complete overlap among the diffusion zones formed around individual electrodes. When the potential deposition is made more negative, E_e= −1.00 V (Figure 2c), a slight increase in the current after approximately 4 s of the beginning of the potentiostatic transient is observed. This can be due to the first stages of iron electrodeposition on the deposited bismuth at this potential, and it can be seen from the stripping voltammogram in Figure 2d, where the appearance of an anodic peak related to the Fe(0) → Fe(II) reaction is detected. The same effect is more clearly observed when the step potential is made even more cathodic, E_e = −1.20 V (see Figure 2e), where a clear nucleation and growth phenomena appears associated with the consecutive electrodeposition of iron, and in agreement with the increase of the stripping charge (see Figure 2f). The Faradaic efficiency during electrodeposition for the potentiostatic transient shown in Figure 2a is about 65%. When the deposition potential is −1.00 V, the Faradaic efficiency is approximately 72% for the potentiostatic transient, shown in Figure 2c as the first stages of iron electrodeposition on the deposited bismuth. The Faradaic efficiency reaches the highest, 88%, for the potentiostatic transient shown in Figure 2e when the deposition potential is −1.20 V as the consecutive electrodeposition of iron.

To obtain in situ information of the prepared deposits, potentiostatic stripping is performed because this method has been proved to be highly useful for the characterization of the electrodeposited intermetallic compounds or alloys.[18] The electrodeposition potentials are selected according to the previous electrochemical results. At first, the deposits obtained from the 1 μM $Bi(NO_3)_3$−1 μM $FeCl_2$−DMF system at the deposition potential E_e= −1.20 V are analyzed. Different solutions are tested to oxidize the deposits. Figure 3 shows the different stripping curves of the deposits when the stripping was made in 1 μM $Bi(NO_3)_3$−1 μM $FeCl_2$−DMF and 0.1 M LiCl−DMF solutions (Figure 3, curves a, b), and the recorded oxidation curves are similar. Two oxidation peaks are always obtained for the striping of bismuth and iron. Moreover, the stripping results obtained from DMF solution are tested (Figure 3, curve c). Although in this medium the appearance of the oxidation current takes place at more positive potential, there are two oxidation peaks of a similar charge to that recorded in 0.1 M

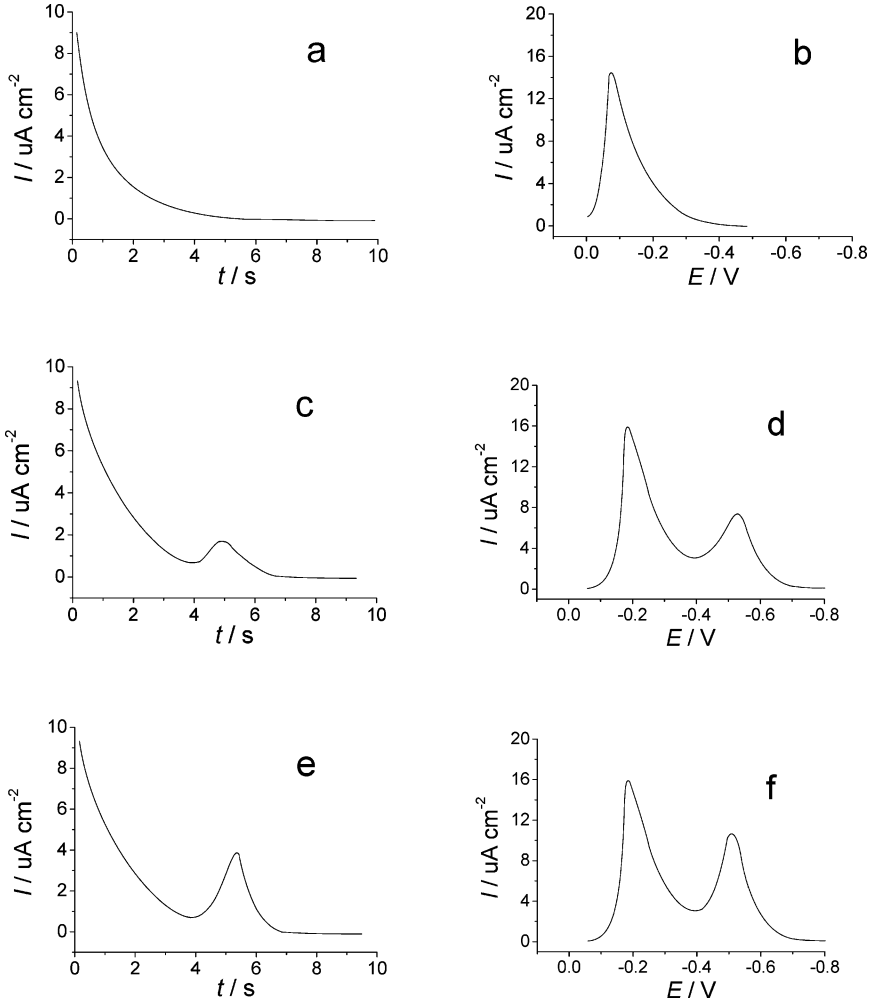

Figure 2. The potentiostatic transients of a polycarbonate membranes in 1 μM $Bi(NO_3)_3$−1 μM $FeCl_2$−DMF solution at potential steps (a) −0.60 V; (c) −1.00 V; (e) −1.20 V. (b), (d), and (f) are the corresponding stripping voltammograms for the intermetallic compounds formed after the potential steps. Scan rate: 0.1 V s^{-1}.

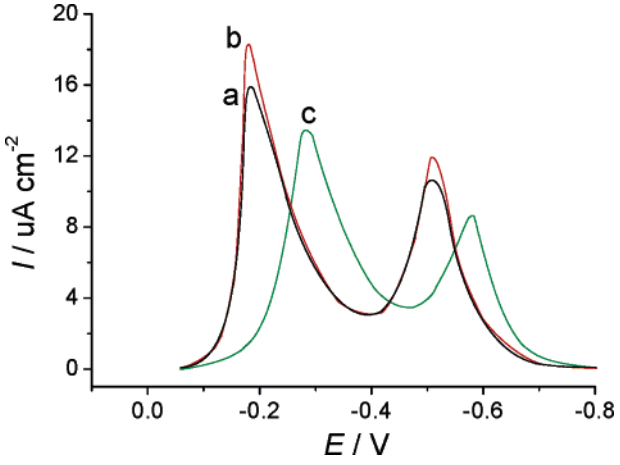

Figure 3. Stripping voltammograms of the deposits obtained from 1 μM $Bi(NO_3)_3$−1 μM $FeCl_2$−DMF solution at the deposition potential $E_e = -1.20$ V in (a) 1 μM $Bi(NO_3)_3$−1 μM $FeCl_2$−DMF; (b) 0.1 mol dm^{-3} LiCl−DMF solution; (c) DMF solution.

LiCl−DMF media. The 0.1 M LiCl−DMF mediums clearly favor deposit oxidation and, therefore, this solution is chosen as a good striping medium because no replacement reaction takes place during the anodic scan. The deposits are prepared when the deposition potential E_e is negative to −2.00 V, and the severe concentration polarization occurs during the deposition. The stripping experiments of these deposits also show two striping peaks, but a clear decrease of the Q_{ox}/Q_{red} ratio is observed, especially when the applied potentials are very negative. Some deposits remain on the electrode after the stripping experiments, revealing that complete oxidation is not attained. Therefore, little qualitative is obtained by using in situ stripping characterization when the deposition potentials are negative to −2.00 V.

The synthesis of $Bi_{1-x}Fe_x$ intermetallic compound nanowire arrays is achieved through electrodepositing Bi and Fe atoms into the membrane pores. In the experiment, the initial potential is increased and the initial current density reaches 0.1 mA/cm^2. The large overpotential is similar to the high saturation degree in the solution, and it can increase the electrochemical polarization and result in the nucleation rate higher than the growth rate. Therefore, during electrodeposition, the more crystal nuclei are generated so as to form a compact and fine structure. As a thin iron layer sputtered on the bottom side of polycarbonate membranes acts as a working electrode before electrodeposition, Fe and Bi atoms will preferentially nucleate and grow, attaching the iron particles from bottom to top when Fe^{2+} and Bi^{3+} are reduced. We observe that the current remains fairly constant when the pores are filling. Nanowires or nanorods can be easily formed by this template method. To obtain the maximum number of wires, nucleation must occur in all of the pores simultaneously. If nucleation occurs rapidly in a few pores, then these pores will fill and growth will continue across the top

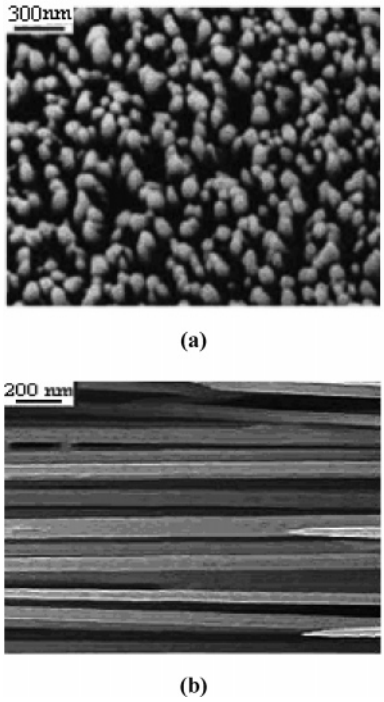

Figure 4. FE-SEM images of the upside (a) and the cross-section (b) of $Bi_{1-x}Fe_x$ intermetallic compounds with nanowire array structure prepared in 1 μM $Bi(NO_3)_3$−1 μM $FeCl_2$−DMF system with electrodeposition potential of −1.2 V at 301 K.

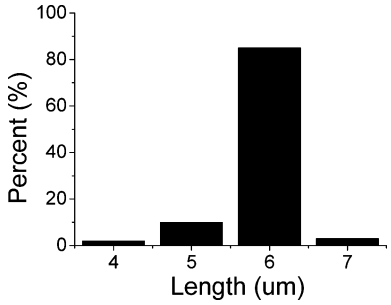

Figure 5. The histogram with the length of the prepared nanowires vs the percent. (The electrodeposition time is 30 min).

surface. So this will block the diffusion of solution down neighboring pores, halting growth. A high degree of nucleation is achieved when current densities are as little as possible, which results in slower growth.

Figure 4 shows the FE-SEM images of the upside and the cross section of $Bi_{1-x}Fe_x$ intermetallic compound nanowire arrays electrodeposited with 0.1 μm pore diameter PC membranes for the plating time of 30 min and an electrodeposition potential of −1.20 V. The diameters of the obtained nanowire arrays are about 80−100 nm. By using current densities that are as little as possible, which results in slower growth, a high degree of nucleation is achieved. At −1.20 V, we observe the nucleation in ∼90% of the pores, as shown in Figure 4a. A FE-SEM image of a cross section of $Bi_{1-x}Fe_x$ intermetallic compound nanowire arrays (Figure 4b) shows that the wires are dense, the average diameters of the obtained nanowire arrays matches closely to the pore size. The diameters of the intermetallic compound nanowire arrays are determined by the sizes of the pores in the polycarbonate membrane. On the other hand, the length of the nanowires varies due to the factors such as electrodeposition time and electrodeposition rate. The histogram with the length of nanowires vs the percent is shown in Figure 5. The length of nanowire arrays can be as long as 5−6 μm,

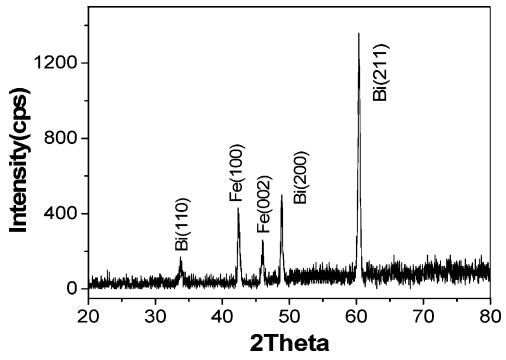

Figure 6. XRD patterns of $Bi_{1-x}Fe_x$ intermetallic compound nanowire arrays prepared in 1 μM $Bi(NO_3)_3$−3 μM $FeCl_2$−DMF system with an electrodeposition potential of −1.20 V at 301 K.

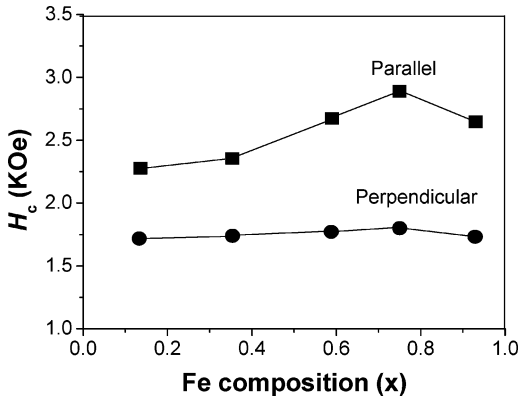

Figure 7. Fe content (x) dependence of coercivity of the as-deposited $Bi_{1-x}Fe_x$ intermetallic compound nanowires measured with the magnetic field applied parallel and perpendicular to the wires at 300 K, respectively.

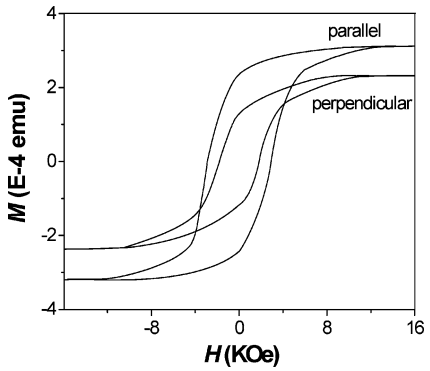

Figure 8. Hysteresis loops of the prepared $Bi_{1-x}Fe_x$ intermetallic compound nanowire arrays at room temperature ($x = 0.75$).

and the degree of uniformity of the length of the nanowires is about 85%. The EDS result shows that the $Bi_{1-x}Fe_x$ intermetallic compound nanowire arrays consist of iron and bismuth, and the compositions of the obtained Bi_xFe_{1-x} intermetallic compound are most sensitive to the concentrations of $Bi(NO_3)_3$ and $FeCl_2$ salts in the deposition solution. For electrolyte compositions of 2 μM $Bi(NO_3)_3$/1 μM $FeCl_2$, and for a range of electrodeposition potential, the resulting $Bi_{1-x}Fe_x$ intermetallic compounds have a low Fe content (10−20 atom % Fe), as determined by EDS. By tuning the solution composition to 1 μM $Bi(NO_3)_3$/3 μM $FeCl_2$, we are able to increase the Fe content of the intermetallic compounds to 50−60 atom %, and the range is predicted to give a large characteristic time of magnetic efficiency. The compositions of $Bi_{1-x}Fe_x$ intermetallic compound nanowire arrays could also be easily adjusted by varying

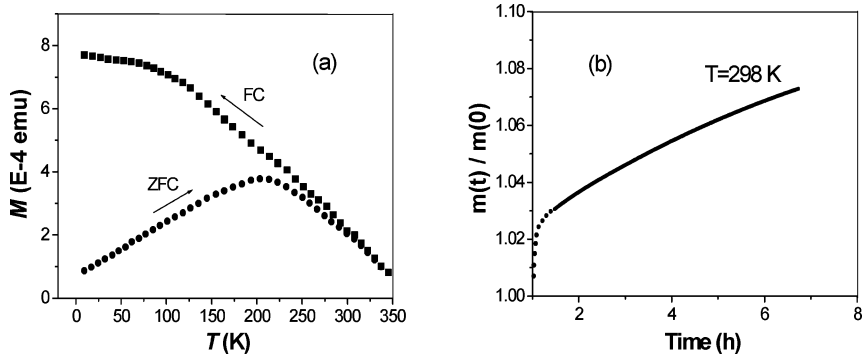

Figure 9. (a) The zero-field-cooled (ZFC) and field-cooled (FC) magnetization curves for $Bi_{1-x}Fe_x$ intermetallic compound nanowire arrays. (b) The normalized magnetization as a function of time for $Bi_{1-x}Fe_x$ intermetallic compound nanowire arrays at 298 K ($x = 0.55$).

electrodeposition potential. With the negative shift of electrodeposition potential, the contents of Fe in $Bi_{1-x}Fe_x$ intermetallic compounds increase at first and then decrease. When the electrodeposition potential is about -1.6 V, the content of Fe in $Bi_{1-x}Fe_x$ intermetallic compounds reaches the highest quantity.

A representative X-ray diffraction pattern for $Bi_{1-x}Fe_x$ intermetallic compound nanowire arrays obtained in the pores of the polycarbonate membrane is shown in Figure 6. The X-ray spectra show the presence of two phases in the deposits. The peaks indicated as Bi shown in Figure 6 are slightly shifted to larger *d* spacing as compared with those of pure Bi, which is consistent with the formation of a solid solution. However, Fe and Bi are immiscible in the equilibrium states, and neither alloy nor intermetallic compound exists in the binary system. The reason such a solid solution $Bi_{1-x}Fe_x$ can be formed by the electrodeposition method under room temperature may be that the co-deposition of Bi^{3+} and Fe^{2+} happens when the electrodeposition potential is negative to -1.20 V.

Figure 7 shows the Fe content dependence of coercivity (H_c) for the electrodeposited $Bi_{1-x}Fe_x$ intermetallic compound nanowire arrays measured at 300 K. It can be clearly seen that all the selected samples have a parallel-to-the-wire easy magnetization. When the magnetic field applied is parallel to the wire, the H_c increases with the increase of Fe content and reaches its maximum at $x = 0.75$ and then decreases. When the magnetic field applied is perpendicular to the wire, the H_c shows little changes with the change of Fe content. To see the magnetization properties clearly, the hysteresis loops of $Bi_{0.25}Fe_{0.75}$ measured at 300 K, with field applied parallel and perpendicular, respectively, to the wire axis, are shown in Figure 8. One can see that $Bi_{0.25}Fe_{0.75}$, which has the higher H_c, shows an H_c of 2.89 KOe with applied field parallel to the wire axis, and the H_c decreased to 1.80 KOe with the applied field perpendicular to the wire, showing a dominating field parallel to the wire easy magnetization.

The field-cooled (FC) and zero-field-cooled (ZFC) magnetization curves of $Bi_{1-x}Fe_x$ intermetallic compound nanowire arrays in a small field of 100 Oe are shown in Figure 9a. The ZFC magnetization increases as the temperature rises from 9 K. When the temperature approaches 207 K, the magnetization reaches a maximum then starts to decrease. The FC magnetization shows its maximum at 9 K and steadily decreases with the temperature increase. Starting at around 298 K, the magnetizations from the ZFC and FC measurements overlap with each other. This observation is consistent with the behaviors of the spin-glass materials, and the freezing temperature (T_f) is about 207 K.

The magnetization process of $Bi_{1-x}Fe_x$ intermetallic compound nanowire arrays under 100 Oe at 298 K is shown in Figure 9b. The experimental data on the solid line in Figure 9b fits with a "stretched" exponential equation $m(t) = m_s - B \exp[-(t/\tau)^{\beta}]$, and $\tau = 5.26$ h and $\beta = 0.48$ can be calculated. The spin-glass system with such a large characteristic time is unusual at room temperature. This unusually large relaxation time may be the result of the special structure of Bi and Fe atoms in the $Bi_{1-x}Fe_x$ intermetallic compound nanowire arrays. The Fe electronic structure could be affected by the large spin−orbit splitting of the circumambient Bi due to the hybridization effect. So the localized Fe spins cannot relax their energy to the system continuously. In other words, the discrete and large energy gap makes the relaxation unusually slow.

4. Conclusions

In summary, this paper presents some results that, by using the nanometer-scale template-based synthesis in conjunction with electrochemical deposition, it is possible to mix in solid solution elements that are immiscible in traditional fabrication methods. The electrochemical method is a simple and efficient path to prepare $Bi_{1-x}Fe_x$ intermetallic compounds with nanowire array structure, and it is expected to be used in other systems that can be electrodeposited. The magnetic measurement of $Bi_{1-x}Fe_x$ intermetallic compound nanowire arrays shows a spin-glass-like behavior, and an unusually large characteristic time that is about 5.26 h is obtained at room temperature.

Acknowledgment. This work was supported by the Kaisi Fellowship, and we thank Dr. Pranavan Salunke for polishing the English in our manuscript.

References and Notes

(1) Yang, F. Y.; Liu, K.; Hong, K.; Reich, D. H.; Searson, P. C.; Chien, C. L. *Science* **1999**, *284*, 1335.

(2) Smith, G. E.; Baraff, G. A.; Rowell, J. M. *Phys. Rev.* **1964**, *135*, A1118.

(3) Komnik, Y. F.; Bukhshtab, E. I.; Nikitin, Y. V.; Andrievskii, V. Z. *Eksp. Teor. Fiz.* **1971**, *60*, 669.

(4) Saitou, M.; Yamaguchi, R.; Oshikawa, W. *Mater. Chem. Phys.* **2002**, *73*, 306.

(5) Monteiro, O. C.; Nogueira, H. I. S.; Trindade, T.; Motevalli, M. *Chem. Mater.* **2001**, *13*, 2103-2111.

(6) Hava, S.; Sequiera, H. B.; Hunsperger, R. G. *J. Appl. Phys.* **1985**, *58*, 1727.

(7) Prieto, A. L.; Sander, M. S.; Martin-Gonzalez, M.; Gronsky, R.; Sands, T.; Stacy, A. M. *J. Am. Chem. Soc.* **2001**, *123*, 7160−7161.

(8) Harada, Y.; Nakanishi, Y.; Yoshimoto, N.; Daibo, M.; Nakamura, M.; Yoshizawa, M. *Physica B* **2003**, *329*−*333*, 1109−1110.

(9) Jin, C.; Xiang, X.; Jia, C.; Liu, W.; Cai, W.; Yao, L.; Li, X. *J. Phys. Chem. B* **2004**, *108*, 1844−1847.

(10) Martin-Gonzalez, M.; Snyder, G. J.; Prieto, A. L.; Gronsky, R.; Keyani, R.; Sands, T.; Stacy, A. M. *Nano Lett.* **2003**, *3*, 973−997.

(11) Li, L.; Li, G.; Zhang, Y.; Yang, Y.; Zhang, L. *J. Phys. Chem. B* **2004**, *108*, 19380−19383.

(12) Prieto, A. L.; Martin-Gonzalez, M.; Keyani, R.; Sands, T.; Stacy, A. M. *J. Am. Chem. Soc.* **2003**, *125*, 2388−2389.

(13) Jin, C. G.; Jiang, G. W.; Liu, W. F.; Cai, W. L.; Yao, L. Z.; Yao, Z.; Li, X. G. *J. Mater. Chem.* **2003**, *13*, 1743−1746.

(14) Martin-Gonzalez, M.; Prieto, A. L.; Knox, M. S.; Gronsky, R.; Sands, T.; Stacy, A. M. *Chem. Mater.* **2003**, *15*, 1676−1681.

(15) Martin, C. R. *Science* **1994**, *266*, 1961.

(16) Martin, C. R. *Chem. Mater.* **1996**, *8*, 1739.

(17) Wang, J.; Tian, M.; Mallouk, T. E.; Chan, M. H. W. *J. Phys. Chem. B* **2004**, *108*, 841−845.

(18) Gómez, E.; Vallés, E. *J. Appl. Electrochem.* **1999**, *29*, 805.